Annals of Biomedical Engineering, Vol. 34, No. 5, May 2006 *(© 2006)* pp. 879–892
DOI: 10.1007/s10439-005-9065-5

Role of Endosomal Trafficking Dynamics on the Regulation of Hepatic Insulin Receptor Activity: Models for Fao Cells

SHARON S. HORI,[1] IRWIN J. KURLAND,[2] and JOSEPH J. DISTEFANO, III[1]

[1] Biocybernetics Laboratory, Departments of Computer Science and Medicine and Biomedical Engineering Interdepartmental Program, University of California, Los Angeles, CA and [2] Departments of Medicine, Pharmacological Sciences and Physiology and Biophysics, SUNY, Stony Brook, NY

(Received 19 August 2005; accepted 7 November 2005; published online: 29 April 2006)

Abstract—Evidence indicates that endosomal insulin receptor (IR) trafficking plays a role in regulating insulin signal transduction. To evaluate its importance, we developed a series of biokinetic models for quantifying activated surface and endosomal IR dynamics from published experimental data. Starting with a published two-compartment Fao hepatoma model, a four-pool model was formulated that depicts IR autophosphorylation after receptor binding, IR endosomal internalization/trafficking, insulin dissociation from and dephosphorylation of internalized IR, and recycling of unliganded, dephosphorylated IR to the plasma membrane. Quantification required three additional data sets, two measured, but unmodeled by the same group. A five-pool model created to include endosomal trafficking of the nonphosphorylated insulin-IR complex was fitted using the same data sets, augmented with another published data set. Creation of a six-pool model added the physiologically relevant dissociation of insulin ligand from the activated endosomal IR. More importantly, all three models, validated against additional data not used in model fitting, predict that, mechanistically, internalization of activated IR is a rate-limiting step, at least under the receptor saturating conditions of the fitting data. This rate includes the transit time to a site where insulin dissociation from and/or dephosphorylation of the IR occurs by docking with protein-tyrosine phosphatases (PTPases), or where a sufficient conformational change occurs in the IR, perhaps due to insulin-IR dissociation, where associated PTPases may complete IR dephosphorylation. Our new models indicate that key events in endosomal IR trafficking have significance in mediating IR activity, possibly serving to regulate insulin signal transduction.

Keywords—Insulin receptor, Insulin signaling, Receptor endocytosis, Receptor recycling, Mathematical model, Parameter estimation.

INTRODUCTION

The insulin receptor (IR) is an integral membrane glycoprotein consisting of two α- and two β-subunits linked by disulfide bonds. The extracellular α-subunits (135 kDa) contain the binding sites for insulin, while the transmembrane β-subunits (95 kDa) contain tyrosine kinase domains that undergo autophosphorylation.[9,30] In the absence of insulin, the extracellular α-subunits inhibit IR activation.[36] Binding of insulin to the α-subunit creates a conformational change in the IR, causing autophosphorylation of the β-subunits.[36] The tyrosine-phosphorylated IR is then internalized via endosomes. The endosomal acidic environment (pH ~6) promotes ligand-receptor dissociation,[13] as well as a conformational dependent inactivation of the IR.[17] Insulin is degraded within the endosome by an acidic insulinase,[2,19] and the IR is either sent to lysosomes for degradation or recycled to the plasma membrane for another round of binding, activation, and internalization.[31]

Receptor-mediated endocytosis is a common cellular mechanism for adjusting the amount of insulin in plasma or the number of receptors on the cell surface.[32] Endocytosis also allows a phosphorylated IR to activate intracellular substrates distal to the plasma membrane,[12] thus initiating a signaling cascade that promotes energy storage/conservation via formation of glycogen and fatty acids (Fig. 1). Activation of the hepatic IR kinase and modulation of key insulin signaling effectors occur at the cell surface, and within the endosomal system.[7,8] Modulation of the acidic environment in endosomes affects both IR recycling and insulin signaling, implying that insulin endosomal receptor trafficking plays a role in regulating insulin signal transduction.[8]

Our goal in this work was to gain a better understanding of the dynamics of IR trafficking, in particular the movement of the IR, from its activation on the cell surface to its deactivation by intracellular protein tyrosine phosphatases. To address this problem, we have extended an existing Fao hepatoma cell model[4] and created three new models, incorporating additional mechanistic structure, which explicitly depicts estimable parameters representing trafficking events associated with the activated and nonactivated IR post-insulin binding. We estimated these new parameters from existing data and have uncovered a rate-limiting step along one of the paths modeled in the IR trafficking subsystem for insulin signaling. We also generated additional

Address correspondence to Sharon S. Hori, Biocybernetics Laboratory, 4532 Boelter Hall, Department of Computer Science, UCLA,Los Angeles,CA 90095-1596. Electronic mail: sharon.hori@ucla.edu.

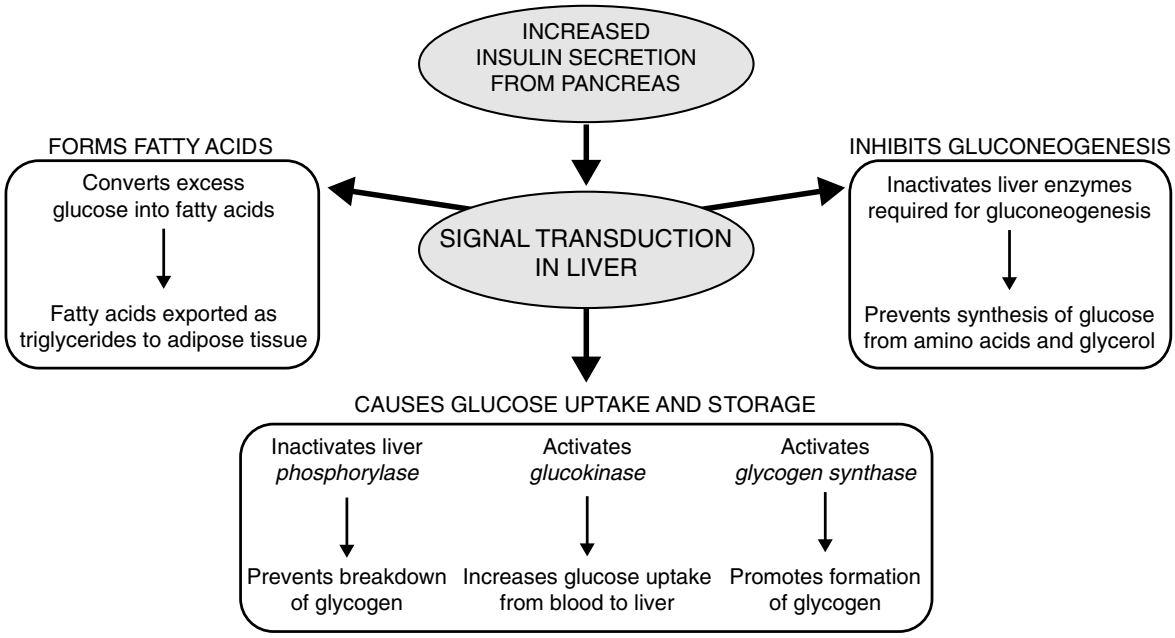

FIGURE 1. Role of insulin signal transduction in hepatocytes.

predictions about IR behavior under normal and insulin resistant conditions, for bound and unbound, phosphorylated and nonphosphorylated, surface and intracellular pools. The three models developed here can be helpful in exploring the dynamics between intracellular and surface IRs for better understanding insulin action at various steps of endosomal trafficking.

MATERIALS AND METHODS

Model Development

Experimental studies that elucidate rates of insulin receptor internalization and recycling have been reported, with either no insulin, or saturating levels of insulin (100 nM) present.[4] The two-compartment IR trafficking model used by Backer and coworkers was the first to be fitted to any experimental data and established the first parameter estimates for the rates of IR internalization and recycling under unbound and saturating conditions.[4] This model, however, did not explicitly include IR phosphorylation or dephosphorylation, now known to be key events in insulin signal transduction. Quon and Campfield[38] created a three state variable model that incorporated insulin bound and unbound IR endocytosis, as well as IR synthesis and degradation. These authors chose literature values for some rate constants and used a heuristically set degradation rate, allowing them to simulate maximal down- and upregulation of the IR. An updated version of this model included IR activation and deactivation mechanisms at saturating conditions, but once again relied on published literature values and boundary conditions—not fits of the model to data—to generate predictive simulations.[42]

In the present study, we take a different approach to modeling and data analysis, using several models of increasing complexity, all fitted to the same temporal kinetic data for IR internalization used originally in Backer *et al.*[4] as well as additional data reported, and not modeled.[4,5,44] We extend the two-compartment Backer *et al.* model,[4] by incorporating receptor activation and deactivation, bound-nonphosphorylated IR trafficking, and insulin dissociation from and dephosphorylation of the internalized IR (Fig. 2). We describe the dynamics of this overall problem by a general model structure valid for any insulin concentration (Fig. 3). Under saturating levels of insulin, this general model reduces to a four-pool model [Fig. 4(a)]. By adding a pool to incorporate trafficking of nonphosphorylated IRs, we created a five-pool model that provides an estimate of the internalization rate of bound-nonphosphorylated IRs [Fig. 4(b)]. We also created a six-pool model, to account for insulin dissociation from the internalized IR [Fig. 4(c)].

For the most general model structure (Fig. 3), we begin at the plasma membrane, where insulin (input u) binds to an unbound surface IR (x_1) to yield a bound surface IR (x_2). Because ligand binding induces receptor activation, the bound surface IR undergoes autophosphorylation to become a bound-phosphorylated surface IR (x_3). Bound-phosphorylated surface IRs undergo endocytosis toward a pool of bound-phosphorylated internalized IRs (x_4). Insulin dissociates from the bound-phosphorylated internalized IR and receptor dephosphorylation occurs, resulting in an unbound internalized IR (x_5). Finally, the unbound internalized IR is recycled to the plasma membrane. See Appendix for definitions and units of all symbolic nomenclature used

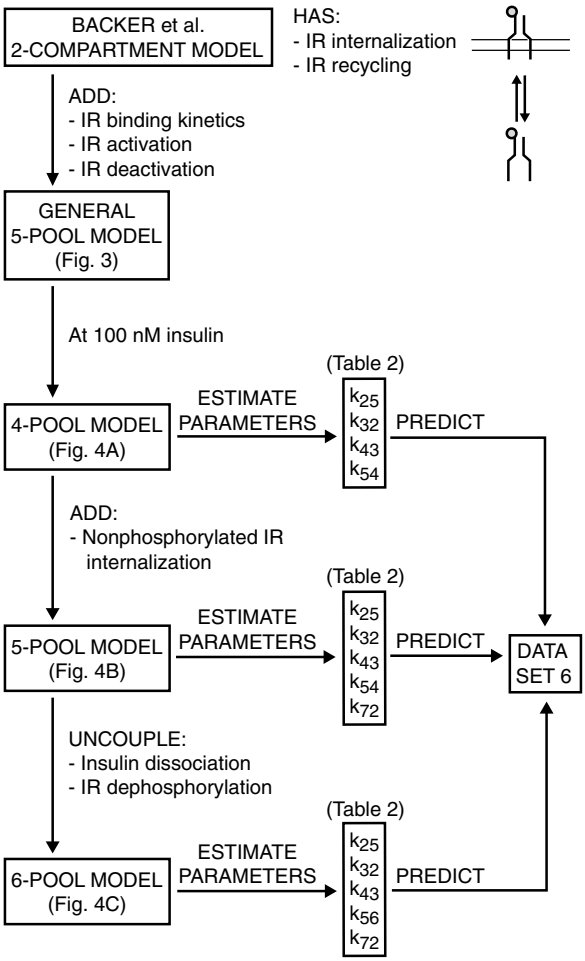

FIGURE 2. Flow chart of model development.

in this paper. The general model equations are

$$u = \text{insulin concentration input}$$

$$\frac{dx_1}{dt} = k_{12}x_2 + k_{15}x_5 - (k_{21}u + k_{51})\,x_1 \tag{1}$$

$$\frac{dx_2}{dt} = k_{21}ux_1 - (k_{12} + k_{32})\,x_2 \tag{2}$$

$$\frac{dx_3}{dt} = k_{32}x_2 - k_{43}x_3 \tag{3}$$

$$\frac{dx_4}{dt} = k_{43}x_3 - k_{54}x_4 \tag{4}$$

$$\frac{dx_5}{dt} = k_{51}x_1 + k_{54}x_4 - k_{15}x_5. \tag{5}$$

The model of Sedaghat *et al.*[42] includes cell surface dephosphorylation mechanisms, allowing a bound-phosphorylated surface IR to return to a bound-nonphosphorylated state. We neglect them here, because the IR does not have intrinsic phosphatase activity[28] and protein tyrosine phosphatase 1B (PTP-1B), mainly responsible for receptor dephosphorylation, has been shown to be

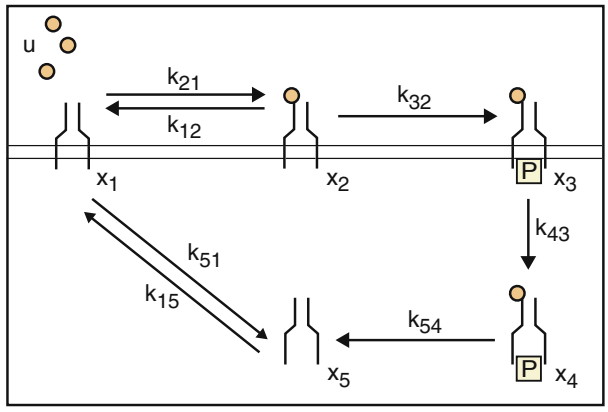

FIGURE 3. General five-pool model of IR binding, autophosphorylation, internalization, deactivation, and recycling. State variables (in percentage of total IR) are defined as follows: x_1 = unbound surface IR, x_2 = bound surface IR, x_3 = bound-phosphorylated surface IR, x_4 = bound-phosphorylated internalized IR, x_5 = unbound internalized IR. Rate constants are defined as follows: k_{12} = dissociation of insulin from bound surface IR (nM^{-1} min^{-1}), k_{21} = association of insulin and unbound surface IR (min^{-1}), k_{32} = phosphorylation of bound surface IR (min^{-1}), k_{43} = internalization of bound-phosphorylated surface IR (min^{-1}), k_{54} = dissociation of insulin from and dephosphorylation of bound-phosphorylated internalized IR (min^{-1}), k_{15} = recycling of unbound internalized IR (min^{-1}), k_{51} = internalization of unbound surface IR (min^{-1}).

located near the endoplasmic reticulum.[25,26] After a 30-min period of insulin saturation, phosphorylated internalized IRs have been shown to undergo dephosphorylation prior to their return to the surface.[4] Since the rate of retroendocytosis of the receptor-ligand complex is negligible in Fao cells,[4] a bound-phosphorylated internalized IR should be deactivated and recycled, as depicted in Fig. 3. Thus, we believe our general five-pool model depicts the minimal requirements to account for IR autophosphorylation, internalization, dephosphorylation, and recycling under a constant level of plasma insulin.

Each reaction is enzymatic and we assume it obeys Michaelis–Menten kinetics. We further assume that, for each state variable x_j, the K_m of the reaction is such that $K_m \gg x_j$, and therefore $k_{ij} = \frac{V_{max}x_j}{K_m + x_j} \approx \frac{V_{max}}{K_m}x_j$ and each reaction rate is assumed linear. Given that our linear models reproduce the data well, this assumption of first-order kinetics appears justified. We note that, however, if $K_m \ll x_j$, then $k_{ij} = \frac{V_{max}x_j}{K_m + x_j} \approx V_{max}$ and the rates may be constant.

When insulin is not present, state variables x_2, x_3, and x_4 are essentially zero and the model collapses into the Backer *et al.* two-compartment model of IR internalization and recycling in the absence of insulin.

Four-Pool Model at 100 nM Insulin

The K_D for the insulin-IR binding interaction has been experimentally determined to be 400 pM.[24] Thus, by maintaining saturating levels of 100 nM insulin, we assume that

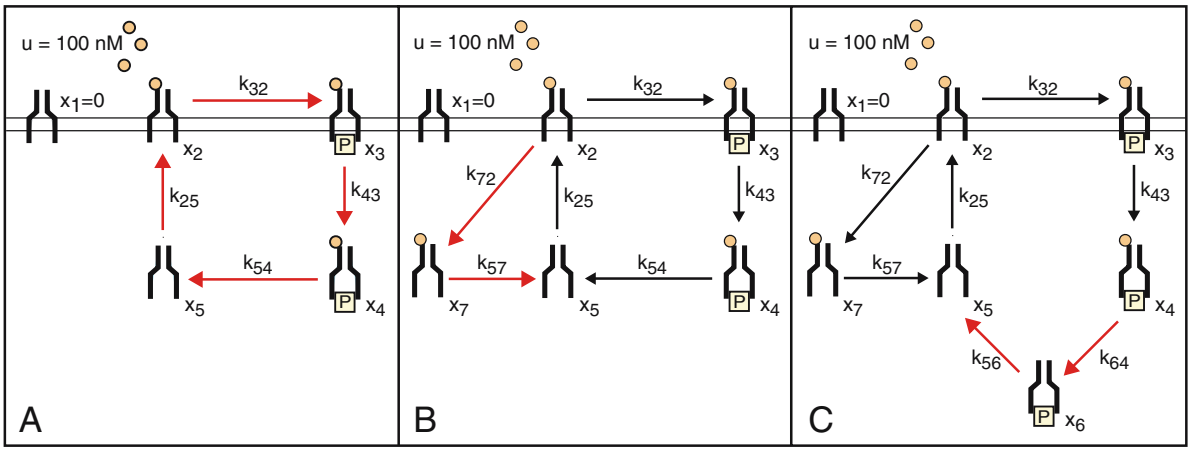

FIGURE 4. Our three models of insulin receptor activation and trafficking under saturating insulin levels (100 nM). (A) Four-pool model of IR autophosphorylation (k_{32}), internalization (k_{43}), deactivation (k_{54}), and recycling (k_{25}). (B) Five-pool model, which also includes the internalization of bound-nonphosphorylated IR (k_{72}) and subsequent dissociation of insulin ligand (k_{57}). (C) Six-pool model, which uncouples IR deactivation into insulin dissociation (k_{64}) and IR dephosphorylation (k_{56}). State variables, rate constants, and initial conditions are defined in Appendix.

the percentage of IRs unbound and at the surface (x_1) is 0 and the percentage of IRs bound and at the surface (x_2) is 100 [Fig. 4(a)], resulting in a four-pool model. Because unbound surface IRs are negligible, we do not consider their internalization. Backer and coworkers showed that the total number of IRs remains constant in these saturation experiments, allowing the assumption that IR degradation is negligible in their two-compartment model. Here we make the same assumption, implying that IR synthesis and degradation rates are approximately equal.[4] The four-pool model equations for saturating conditions are

$$u = 100\,\text{nM insulin input}$$

$$\frac{dx_1}{dt} = 0 \tag{6}$$

$$\frac{dx_2}{dt} = k_{25}x_5 - k_{32}x_2 \tag{7}$$

$$\frac{dx_3}{dt} = k_{32}x_2 - k_{43}x_3 \tag{8}$$

$$\frac{dx_4}{dt} = k_{43}x_3 - k_{54}x_4 \tag{9}$$

$$\frac{dx_5}{dt} = k_{54}x_4 - k_{25}x_5. \tag{10}$$

By using data sets 1, 2, 3, and 4, described later, we generated the following measurement model to be used for data fitting, where y_i represents the output equation corresponding to data set i:

$$y_1 = x_3 + x_4 \tag{11}$$

$$y_2 = x_4 + x_5 \tag{12}$$

$$y_3 = x_2 + x_3 \tag{13}$$

$$y_4 = \frac{x_4}{x_4 + x_5} \times 100. \tag{14}$$

Here y_1 is the percentage of total cellular IRs (surface and intracellular) that are phosphorylated, y_2 is the percentage of total cellular IRs that are internalized, y_3 is percentage of total cellular IRs on the cell surface, and y_4 is percentage of internalized IRs that are phosphorylated.

Five-Pool Model at 100 nM Insulin

Tyrosine phosphorylation of the IR does not appear to be required for internalization.[5] We therefore extended the four-pool model by including the internalization (k_{72}) of bound-nonphosphorylated surface IRs to an intracellular pool (x_7), from which insulin dissociates, resulting in an unbound internalized IR (x_5) [Fig. 4(b)]. In this five-pool model, we also assume that only unbound IRs can be recycled, so that the ligand must first dissociate from the nonphosphorylated IR before the IR is translocated to the membrane. The five-pool model equations for saturating conditions are

$$u = 100\,\text{nM insulin}$$

$$\frac{dx_1}{dt} = 0 \tag{15}$$

$$\frac{dx_2}{dt} = k_{25}x_5 - (k_{32} + k_{72})\,x_2 \tag{16}$$

$$\frac{dx_3}{dt} = k_{32}x_2 - k_{43}x_3 \tag{17}$$

$$\frac{dx_4}{dt} = k_{43}x_3 - k_{54}x_4 \tag{18}$$

$$\frac{dx_5}{dt} = k_{54}x_4 + k_{57}x_7 - k_{25}x_5 \tag{19}$$

$$\frac{dx_7}{dt} = k_{72}x_2 - k_{57}x_7. \tag{20}$$

We included data set 5 in data fitting, and generated the following measurement model:

$$y_1 = x_3 + x_4 \tag{21}$$

$$y_2 = x_4 + x_5 + x_7 \tag{22}$$

$$y_3 = x_2 + x_3 \tag{23}$$

$$y_4 = \frac{x_4}{x_4 + x_5 + x_7} \times 100 \tag{24}$$

$$y_5 = x_5 + x_7, \tag{25}$$

where y_5 is the percentage of total cellular IRs that are internalized and nonphosphorylated, and y_1, y_2, y_3, and y_4 are as previously defined.

Six-Pool Model at 100 nM Insulin

We added another level of complexity to uncouple the process of IR deactivation into distinct steps of insulin dissociation (k_{64}) and IR dephosphorylation (k_{56}) [Fig. 4(c)]. The four- and five-pool models only provide estimates for overall IR deactivation (k_{54}), whereas this six-pool model provides estimates for k_{64} and k_{56}.

It has been shown that the rate of insulin dissociation is approximately the same for bound IRs in endosomes with a pH range from 5.5 to 8.[13] We assume this range for the late endosomal pools x_4 and x_7; thus, $k_{64} \approx k_{57}$, and k_{43} represents the rate at which the phosphorylated IR traverses the plasma membrane and travels through the cytosol to its site of dephosphosphorylation. The six-pool model equations for saturating conditions are

$$u = 100\,\text{nM insulin}$$

$$\frac{dx_1}{dt} = 0 \tag{26}$$

$$\frac{dx_2}{dt} = k_{25}x_5 - (k_{32} + k_{72})\,x_2 \tag{27}$$

$$\frac{dx_3}{dt} = k_{32}x_2 - k_{43}x_3 \tag{28}$$

$$\frac{dx_4}{dt} = k_{43}x_3 - k_{64}x_4 \tag{29}$$

$$\frac{dx_5}{dt} = k_{56}x_6 + k_{57}x_7 - k_{25}x_5 \tag{30}$$

Table 1. Output equations for data sets 1-6.

Data set	Four-pool	Five-pool	Six-pool
1	$x_3 + x_4$	$x_3 + x_4$	$x_3 + x_4$
2	$x_4 + x_5$	$x_4 + x_5 + x_7$	$x_4 + x_5 + x_7$
3	$x_2 + x_3$	$x_2 + x_3$	$x_2 + x_3$
4	$\frac{x_4}{x_4+x_5} \times 100$	$\frac{x_4}{x_4+x_5+x_7} \times 100$	$\frac{x_4+x_6}{x_4+x_5+x_6+x_7} \times 100$
5	–	$x_5 + x_7$	$x_5 + x_7$
6	x_4	x_4	$x_4 + x_6$

$$\frac{dx_6}{dt} = k_{64}x_4 - k_{56}x_6 \tag{31}$$

$$\frac{dx_7}{dt} = k_{72}x_2 - k_{57}x_7. \tag{32}$$

Data sets 1–5 were used for fitting this model, using the following measurement model:

$$y_1 = x_3 + x_4 + x_6 \tag{33}$$

$$y_2 = x_4 + x_5 + x_6 + x_7 \tag{34}$$

$$y_3 = x_2 + x_3 \tag{35}$$

$$y_4 = \frac{x_4 + x_6}{x_4 + x_5 + x_6 + x_7} \times 100 \tag{36}$$

$$y_5 = x_5 + x_7. \tag{37}$$

Biological Data for Model Fitting

We chose to model Fao cell cultures because they possess abundant IRs and display liver-specific properties, e.g., they secrete albumin and synthesize liver isomers of alcohol dehydrogenase and aldolase.[18] State variables were assigned to each data set, as indicated in Table 1.

Data Set 1: Time Course of IR Autophosphorylation

White *et al.*[44] measured the time course of IR autophosphorylation in Fao cells at 22°C. Data set 1 [Fig. 5(a)] was used initially in fitting our four-pool model, and later our five- and six-pool models.

Data Set 2 : Time Course of IR Internalization

Backer *et al.*[4] studied the time course of the appearance of IRs inside Fao cells at 37°C, finding that 30–35% of IRs were internalized within 20 min of saturating insulin stimulation. Data set 2 [Fig. 5(b)] was used in the Backer *et al.* two-compartment model,[4] as well as in our four-, five-, and six-pool models.

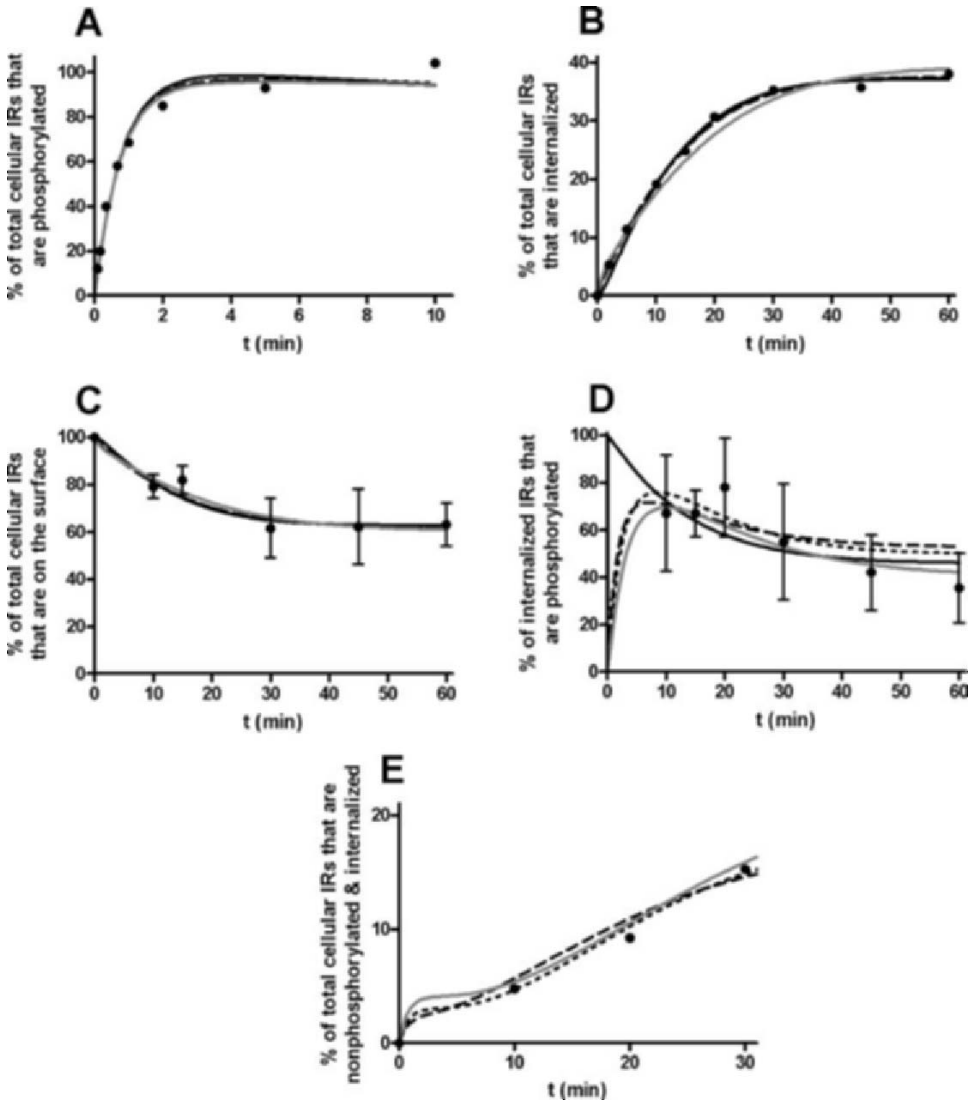

FIGURE 5. Fitting of four-pool (—), five-pool (- - -) and six-pool (· · ·) models to data sets 1–5 using relative weighting. The 6-pool model was also fitted to data sets 1–5 using absolute weighting (solid gray line). Time courses for IR autophosphorylation (A), IR internalization (B), disappearance of surface IRs (C), ratio of phosphorylated internalized IRs to total internalized IRs (D), and nonphosphorylated IR internalization (E) at 100 nM insulin. Figure 5(a)–5(e) correspond to data sets 1–5, respectively. The fits in (A), (B), and (C) indicate no significant difference in the four-, five-, and six-pool models, whereas in (D) the five- and six-pool models fit significantly better by objective (least squares) criteria. In (E), only the five- and six-pool models were fitted to data set 5.

Data Set 3: Insulin-Stimulated Loss of Surface Insulin Binding

Backer *et al.*[4] also examined the rate of IR internalization at 37°C by measuring the time course of the disappearance of cell surface IRs after specified periods of saturating insulin stimulation. Data set 3 [Fig. 5(c)] was used initially in fitting our four-pool model, and later our five- and six-pool models.

Data Set 4 : Time Course of Internalization of Phosphorylated IRs

In the same work, Backer *et al.*[4] examined the time course of the appearance of phosphorylated IRs inside Fao cells at 37°C over a 60-min period. Data set 4 [Fig. 5(d)] was used initially in fitting our four-pool model, and later our five- and six-pool models.

Data Set 5: Insulin-stimulated Internalization of the IR in Control and DNP-Treated Fao Cells

Backer *et al.*[5] showed that tyrosine phosphorylation is not necessary for IR internalization at 37°C. Data set 5 [Fig. 5(e)] was used initially in fitting our five-pool model, and later our six-pool model.

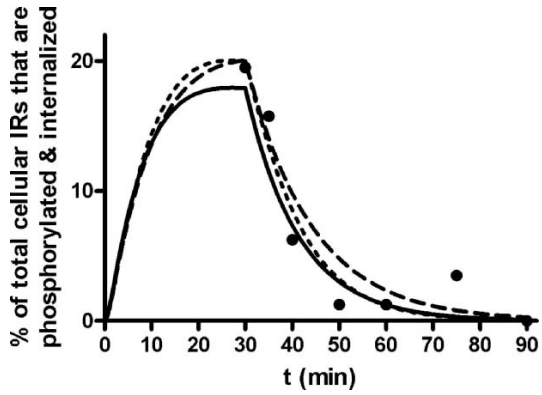

FIGURE 6. Time course for dephosphorylation of internalized IRs during recycling. Predictions were made using four-pool (—), five-pool (- - -), and six-pool (· · ·) models.

Data Set 6: Dephosphorylation of Internalized IRs During Recycling

Backer *et al.*[4] followed the time course of IR recycling at 37°C over a 60-min period after saturating insulin stimulation. Data set 6 (Fig. 6) was not used in any model fitting, but was used to validate predictions of the time course of dephosphorylation of internalized IRs during recycling in our four-, five-, and six-pool models.

Parameter Estimation

Unique structural identifiability of the four-pool model [Fig. 4(a)] was readily established via analysis of the transfer function[16] defined by the model and output Eqs. (6)–(14). Identifiability of the five- and six-pool models [Fig. 4(b) and 4(c)] was established numerically, by examining the covariance matrices for parameter estimates following actual fitting of these models to data, using additional parameter information provided in Backer *et al.*,[3] as described later. Finite and reasonable parameter estimate variances (or % CVs, as in Table 2) assure *a priori* as well as numerical identifiability.[16] The % CVs also provide a measure of parameter sensitivity,[41] with a low parameter CV implying that the model output is very sensitive to changes in the respective parameter value.

Models were fitted to data and parameter estimates were obtained using the program SAAM II,[10] with a Rosenbrock integrator and relative weighting.[10,11] Data sets 1, 2, and 5 were provided without data variability[4,5,44] and the SDs of data sets 3 and 4 were large compared with their mean values.[4] Using an extended least-squares implementation in SAAM II, we included the known SDs of data sets 3 and 4 into the fitting. Extended least squares provides unbiased parameter estimates when data variances are unknown, and its implementation over weighted least squares has been justified previously.[34,35]

Because data set 2 represents the time course of internalized IRs and data set 3 represents the time course of surface IRs, the sum of the two should theoretically be 100% at all times. The sum of these independently derived data sets was 110%, thus requiring normalization to account for inherent errors in experimental methodology.[4] We then fitted each model, as described below.

When comparing different model structures fitted to the same data sets, an improved fit can be due simply to the increase in the number of model parameters. The Akaike information criterion (AIC) is useful in this situation because it penalizes a model for having an increased parameter space, i.e., more degrees of freedom.[1] The AIC is given as $\mathrm{AIC} = N \ln(\mathrm{WRSS}) + 2P$, where N is the number of data points, WRSS is the weighted residual sum of squares, and P is the number of parameters in the model. A lower AIC indicates a better fit to experimental data.

Four-Pool Model at 100 nM Insulin

We fitted all four parameters (k_{25}, k_{32}, k_{43}, k_{54}) of our four-pool model to data sets 1–4.

Table 2. Parameter estimates for four-, five-, and six-pool models.

	Four-pool (AIC = 2.89)			Five-pool (AIC = 2.64)			Six-pool (AIC = 2.52)		
Parameter	Estimate (min^{-1})	T (min)	% CV	Estimate (min^{-1})	T (min)	% CV	Estimate (min^{-1})	T (min)	% CV
k_{25}	0.0762	13.1	11.3	0.0829	12.1	8.44	0.0737	13.6	9.4
k_{32}	1.29	0.775	8.63	1.30	0.769	8.15	1.29	0.775	7.64
k_{43}	0.0247	40.5	4.30	0.0230	43.5	3.68	0.0212	47.2	3.16
k_{54}	0.0893	11.2	10.4	0.0716	14.0	6.09	—	—	—
k_{56}	—	—	—	—	—	—	0.101	9.90	5.76
k_{72}	—	—	—	0.0320	31.25	27.5	0.0411	24.3	18.7

Note. k_{25}: fractional rate (FR) of IR recycling; k_{32}: FR of surface IR autophosphorylation; k_{43}: FR of phosphorylated IR internalization; k_{54}: FR of IR deactivation; k_{56}: FR of internalized IR dephosphorylation; k_{72}: FR of nonphosphorylated IR internalization. $T = 1/k_{ij}$. % CV = 100 × SD/estimate.

Five-Pool Model at 100 nM Insulin

The dissociation rate of insulin from the endosomal IR has been measured with $t_{1/2} = 3$ min,[3] so in our five-pool model we set $k_{57} = (\ln 2)/t_{1/2} = 0.23$ min^{-1}. We fitted the remaining five parameters (k_{25}, k_{32}, k_{43}, k_{54}, k_{72}) to data sets 1–5.

Six-Pool Model at 100 nM Insulin

As described in Model Development section, we fixed $k_{64} = k_{57} = 0.23$ min^{-1}. We estimated the remaining five parameters (k_{25}, k_{32}, k_{43}, k_{56}, k_{72}) using data sets 1–5. To test robustness of our model-data fits to the choice of data error model, we refitted the six-pool model, our most complex representation, to the data using absolute weighting, in which the data variability is assumed known. In our absolute weighting model, we used SD = 10 (up to 200% errors) for data sets 1, 2, and 5, assumedly an upper bound for the unknown SDs of these data means.

RESULTS

Quantified Models and Parameter Estimates

The best fits of the four-, five-, and six-pool models to data sets 1–5 are shown in Fig. 5(a)–5(e). Since all IRs undergoing internalization are initially phosphorylated, the simulation for data set 4 begins at 100% for the four-pool model [Fig. 5(d)]. In the five- and six-pool models, the fits to data set 4 begin at 0%, since the rate of activated IR internalization (k_{43}) is slow relative to the remaining rates (Table 2), and this is bypassed in the five-pool and six-pool models, as IRs can be internalized without being phosphorylated (see Discussion section). Absolute data weighting results were only distinguishable from relative weighting results in data set 4 (Fig. 5). Parameter estimates and their % CVs are given in Tables 2 and 3.

Table 3. Parameter estimates for six-pool model using absolute weighting.

Parameter	Estimate (min^{-1})	T (min)	% CV
k_{25}	0.0465	21.5	54.3
k_{32}	1.31	0.765	16.5
k_{43}	0.0178	56.2	27.3
k_{56}	0.0996	10.0	48.5
k_{72}	0.0535	18.7	10.0

Note. k_{25}: fractional rate (FR) of IR recycling; k_{32}: FR of surface IR autophosphorylation; k_{43}: FR of phosphorylated IR internalization; k_{56}: FR of internalized IR dephosphorylation; k_{72}: FR of nonphosphorylated IR internalization. $T = 1/k_{ij}$. % CV = 100 × SD/estimate.

Four-, Five-, and Six-Pool Model Predictions

We simulated each model using parameter estimates from Table 2 and compared the simulations to data set 6, which was not used in the model fitting process (Fig. 6). Based on experimental conditions given in Backer *et al.*,[4] we set initial conditions $x_2(0) = 100\%$ and $x_3(0) = \cdots = x_7(0) = 0\%$; and at $t = 30$ min, model parameters were set to $k_{32} = k_{43} = 0$ for the four-pool model, and $k_{32} = k_{43} = k_{72} = 0$ for the five-pool and six-pool models (see Data Set 6 section). Figure 6 illustrates reasonably successful prediction of data set 6 by each model.

We showed that our six-pool model is capable of simulating defective states of insulin action, by adjusting the total number of IRs, decreasing the IR autophosphorylation rate, or decreasing the IR internalization rate. Using parameter estimates established for the six-pool model (Table 2), we simulated IR cycling when $x_2(0) = 100$, 90, 60, and 30% of total cellular IRs are present [Fig. 7(a) and 7(b)]. As expected, decreasing the initial amount of IRs available for the cell decreases the total percentage of phosphorylated IRs and phosphorylated internalized IRs, reaching steady-state levels by 20 min. We also simulated 0, 25, 50, and 70% decreases in the rate of IR autophosphorylation, and found that steady-state levels of phosphorylated IR were not affected [Fig. 7(c) and 7(d)]. Finally, we simulated 0, 25, 50 and 70% decreases in the rate of bound phosphorylated IR internalization, and found that the percentage of total phosphorylated IRs decreased significantly only after 10 min, while the percentage of phosphorylated internalized IRs was affected almost immediately [Fig. 7(e) and 7(f)].

For each model, we also predicted the percentage of IRs in each individual pool, $x_2, \ldots, x_7$, representing all forms of surface and intracellular IRs (bound and unbound, phosphorylated and nonphosphorylated) and plotted them over a 60-min period in Fig. 8(a)–8(f). The x_2, x_3, and x_5 predictions are similar for the four-, five-, and six-pool models (Fig. 8(a), 8(b), and 8(d)). For the x_4 prediction, the four and five-pool models reach a steady-state value of 17–20% at about 25 min, while the six-pool model reaches a steady-state value of 7% at 10 min [Fig. 8(c)]. The x_7 prediction is similar for the five- and six-pool models [Fig. 8(e)], and the x_6 prediction was made only for the six-pool model [Fig. 8(f)]. The time course for x_6 suggests the reason for which x_4 is lower in the six-pool model, namely a significant amount of the phosphorylated IR accumulates intracellularly even after loss/degradation of the insulin ligand.

DISCUSSION

Our three new models of IR activation and trafficking describe receptor kinetics at saturating levels of insulin in Fao cells. Together they provide substantially more information about IR internalization and recycling rates

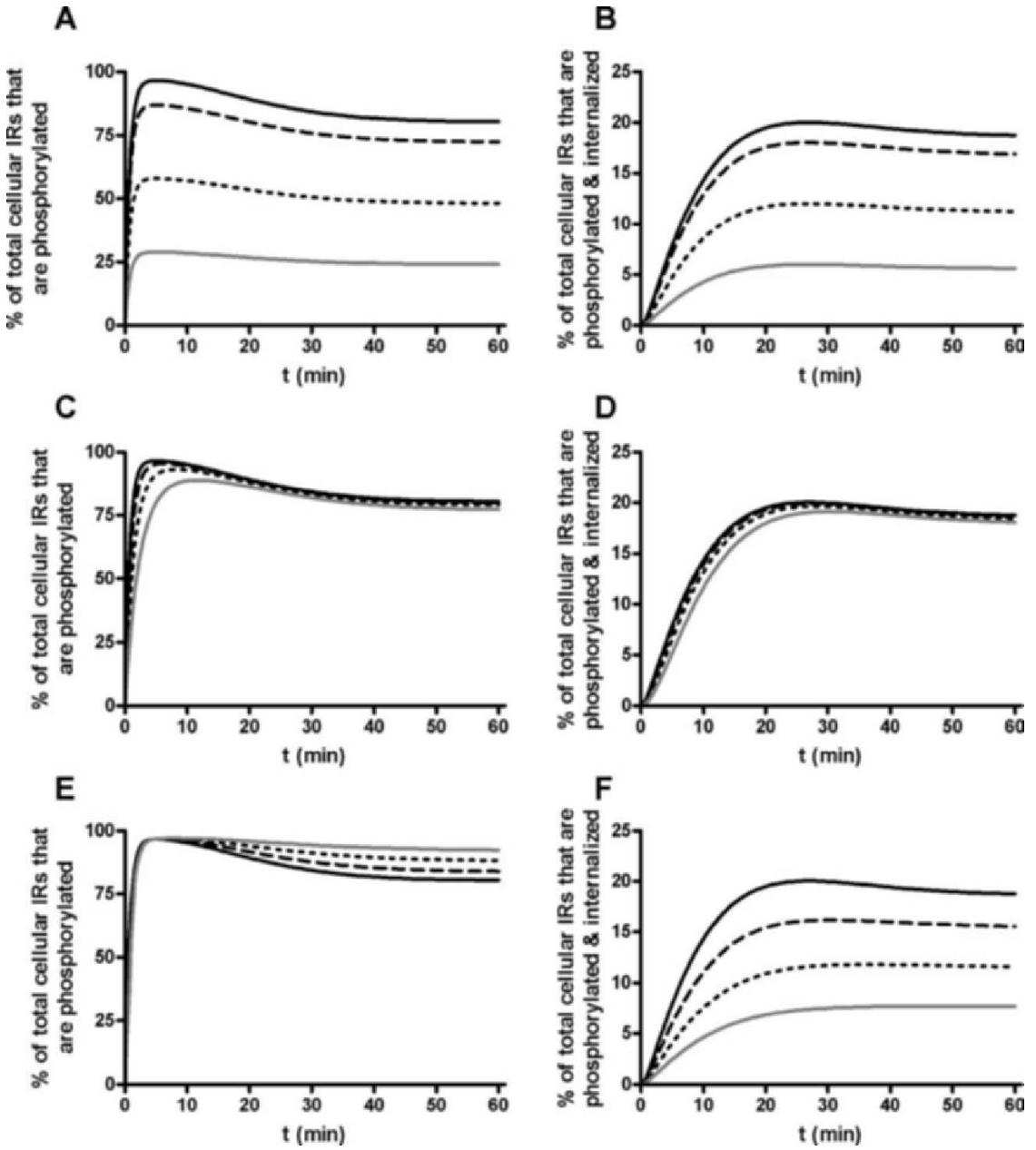

FIGURE 7. Using the six-pool model to simulate cell-associated phosphorylated IRs (A, C, E) and internalized phosphorylated IRs (B, D, F) for insulin resistant conditions, as a percentage of total IR. (A) and (B) show time courses when 100% (—), 90% (- - -), 60% (· · ·), and 30% (solid gray line) of IRs are present. (C) and (D) show time courses when IR autophosphorylation rate is 100% (—), 75% (- - -), 50% (· · ·), and 30% (solid gray line) of its estimated value ($k_{32} = 1.29$ min^{-1}). (E) and (F) show time courses when activated IR internalization rate is 100% (—), 75% (- - -), 50% (· · ·), and 30% (solid gray line) of its estimated value ($k_{43} = 0.0212$ min^{-1}).

than previously reported, plus new estimates for the rates of IR autophosphorylation, dephosphorylation, and insulin dissociation from the activated and nonactivated IR, not previously reported. These four-, five-, and six-pool models balance parameter identifiability with the minimal structural complexity necessary to cover the range of insulin receptor activation/deactivation events that have been experimentally observed. For example, the four-pool model covers the basic framework of insulin autophosphorylation after receptor binding, endosomal trafficking/internalization of the activated insulin receptor, the combined steps of insulin dissociation from and dephosphorylation of the internalized IR, and recycling of the unliganded, dephosphorylated IR to the plasma membrane [Fig. 4(a)]. The five-pool model adds the endosomal trafficking of the nonphosphorylated insulin-IR complex, and

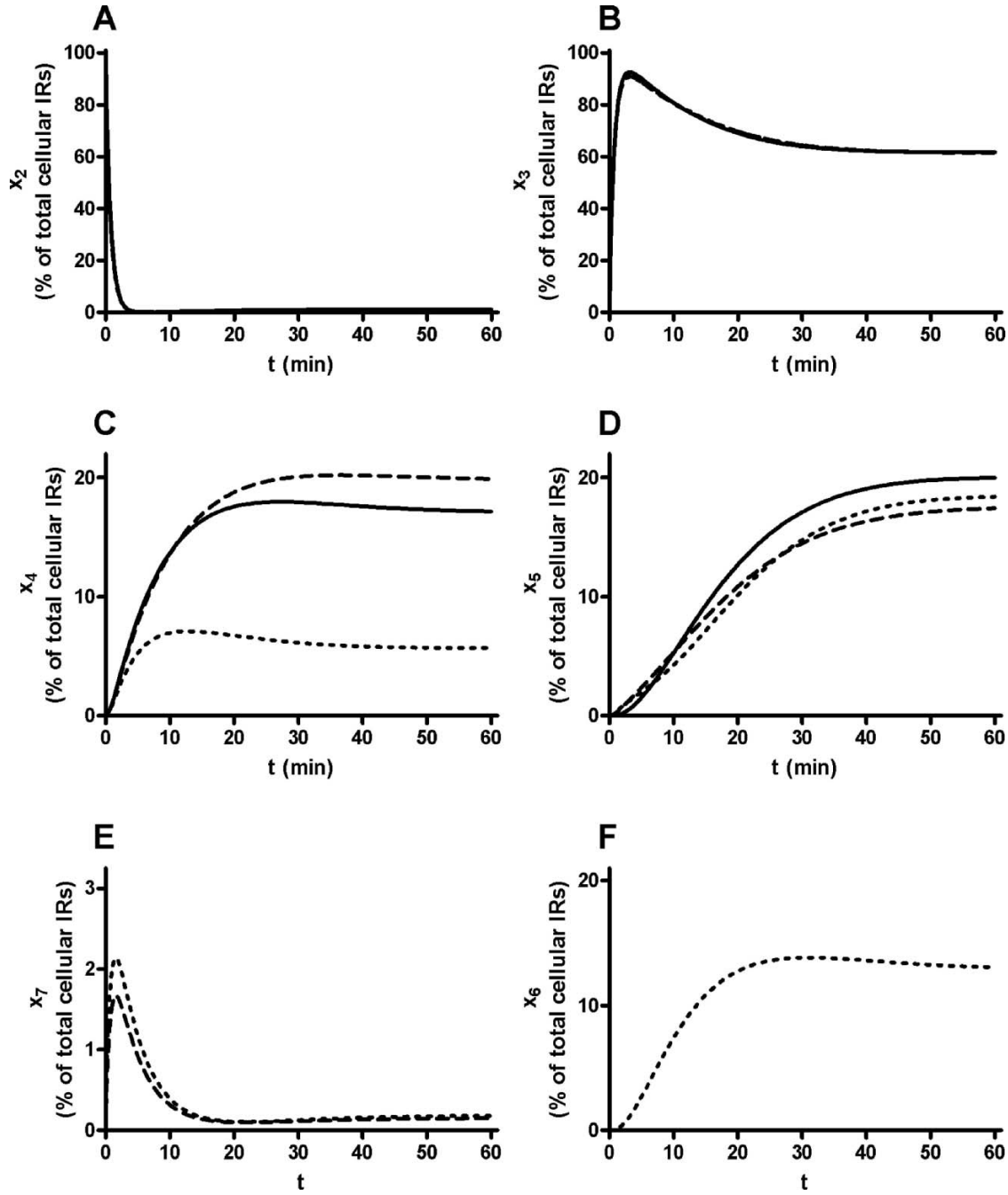

FIGURE 8. Simulations of x_2, bound surface IRs (A); x_3, bound-phosphorylated surface IR pool (B); x_4, bound-phosphorylated internalized IRs (C); x_5, unbound-nonphosphorylated internalized IRs (D); x_7, bound-nonphosphorylated internalized IRs (E); and x_6, unbound-phosphorylated internalized IRs (F), using four-pool (—), five-pool (- - -), and six-pool (· · ·) models.

its recycling back to the PM [Fig. 4(b)]. The six-pool model adds to the five-pool model a description of the physiologically relevant dissociation of the insulin ligand from the activated IR, and the recycling of the phosphorylated unliganded IR back to the PM [Fig. 4(c)].

Importantly, all three new models predict that internalization of the phosphorylated, activated IR (k_{43}) is a rate-limiting step in the IR subsystem modeled here, at least under receptor saturating conditions, the conditions of the fitting data. This rate includes the transit time to a site where insulin dissociation from the IR and/or dephosphorylation of the IR occurs. PTPases are known to be necessary and important in the physiological regulation of the insulin receptor.[15,19,20] Candidate PTPases for terminating insulin

action thought not to have redundant functions include PTP-1B,[27,29,39] TCPTP,[22,23,33] and as yet undefined endosomal associated PTPases.[21,40] The dephosphorylation site may be where PTPases are docked,[25,40] or simply the point in the endosomal trafficking cycle where a sufficient conformational change occurs, perhaps secondary to the loss of insulin from the IR, where endosomal associated PTPase(s) may be able to complete dephosphorylation of the IR. In support of this latter hypothesis, Bevan *et al.*[13] found that promotion of sustained receptor binding decreases endosomal insulin degradation and extends the half-life of the activated endosomal receptor. Contreres *et al.*[17] found that the acidic pH of endosomes fosters a conformation-dependent inactivation of the IR kinase (IRK), and an acidic endosomal insulinase has recently been identified as cathespin D.[2] An understanding of the molecular mechanisms that influence rate-limiting step k_{43} may lead to treatments which could result in its prolongation, possibly increasing insulin sensitivity and improving the condition of insulin resistance in diabetic patients. Posner has suggested that the key to this type of treatment is the identification of molecular targets within the IRK signaling pathway.[37] Such treatments may modulate endosomal processes, e.g., dissociation of insulin or dephosphorylation of the IR, which have been shown to limit the intensity and duration of the intracellular signal transduction.[37]

We recognize that cell-specific differences in the complement of phosphatases and/or differences in the distribution of lipid rafts (localized domains of the cell membrane enriched with specific proteins, sphingolipids and/or cholesterol) within individual tissues might influence targeting and kinetics of receptor-mediated endocytosis. We have chosen to model liver cells first, as opposed to myocytes, because muscle-specific IR knockout mice have nearly normal glucose tolerance, while liver-specific IR knockouts are severely insulin resistant.[14] Creating a valid model in hepatocytes is the first step toward establishment of a model that holds for all cell types.

Four-Pool Model at 100 nM Insulin

Backer and coworkers[4] were the first to explore the fundamentals of IR trafficking. The authors fitted a two-compartment model to their data (at 100 nM insulin) which then provided estimates of IR internalization ($k_{\text{in}} = 0.033\ \text{min}^{-1}$) and recycling ($k_{\text{re}} = 0.048\ \text{min}^{-1}$) rates. We added IR autophosphorylation and IR dephosphorylation to the Backer *et al.* model, to examine the rates of IR activation and deactivation, because these processes are known to be important in insulin signaling.[6,20] By adding a bound-phosphorylated surface IR pool, we separated the surface IR compartment into disjoint activated and nonactivated pools. Similarly, by adding an unbound-nonphosphorylated internalized IR pool, we segregated the internalized IR compartment. We thus added minimal complexity, to ensure robustness and to examine the effects of gradual enhancements.

Our four-pool estimates of the fractional rate of IR internalization ($k_{43} = 0.0247\ \text{min}^{-1}$) and recycling ($k_{25} = 0.0762\ \text{min}^{-1}$) were one-third lower, and one-half higher than the Backer *et al.*[4] estimates (k_{in} and k_{re}, respectively), which we attribute to the increased complexity of our model. Backer and coworkers did not use autophosphorylation data in their model fitting, and thus did not account for IR autophosphorylation as a separate process from IR endocytosis. Hence, the internalization rate k_{in} in the Backer *et al.* model also includes IR autophosphorylation, which we estimated separately. Similarly, the recycling rate k_{re} includes the rate of insulin dissociation and IR dephosphorylation, which we estimated separately, with the addition of data set 4 during model fitting. We cannot provide p-values for these comparisons because no parameter variability estimates were given by Backer *et al.*[4]

We found the fractional rate of IR autophosphorylation ($k_{32} = 1.29\ \text{min}^{-1}$) is over 14 times faster than the combined fractional rates of insulin dissociation and IR dephosphorylation ($k_{54} = 0.0893\ \text{min}^{-1}$), supporting the hypothesis that a slower dephosphorylation rate may accentuate the insulin signaling response.[20] While signaling molecules (PDK, AKT, etc.) may be recruited to the activated surface IR to enhance signaling strength, our model shows that activated IR internalization provides another effective means for the IR to carry out the insulin signal and activate downstream substrates. Furthermore, the slower the rate of IR internalization (k_{43}), the longer the activated IR is capable of phosphorylating downstream substrates, thus extending the period during which the IR can modulate its signal.

The four-pool model is capable of simulating IR activation and deactivation processes, but it does not describe bound-nonphosphorylated surface IR internalization known to occur at saturating insulin conditions.

Five-Pool Model at 100 nM Insulin

Knowing that the IR can be internalized without undergoing autophosphorylation, we separately rendered the rates of activated and nonactivated receptor endocytosis in our five-pool model, by dividing the nonphosphorylated internalized IR pool of the four-pool model (i.e., x_5) into distinct IR pools with insulin bound and unbound. The new pool for bound-nonphosphorylated internalized IRs (x_7) represents insulin sequestered by IRs that are unable to carry out the insulin signal.

We found that nonphosphorylated IR internalization ($k_{72} = 0.0320\ \text{min}^{-1}$) is about 70% faster than phosphorylated IR internalization ($k_{43} = 0.0230\ \text{min}^{-1}$), but both rates are slow relative to the remaining activation and trafficking parameters. This again suggests that phosphorylated IR internalization is a rate-limiting step under saturating

insulin conditions, allowing an extended period of time for phosphorylated IR to activate intracellular downstream substrates. We note that under subsaturating insulin conditions, trafficking rates may differ and phosphorylated IR internalization may no longer be the slowest step, relative to the remaining trafficking processes.

Interestingly, since nonphosphorylated IRs cannot carry out the insulin signal,[40] the x_7 pool serves to cycle IRs not involved in signaling. However, this access route, and the faster internalization rate identified for k_{72} vs. k_{43}, results in a dramatically different prediction of the early time course for the percentage of internalized IRs phosphorylated [Fig. 5(d)]. The early time course predicted for models having k_{72} shows an upswing in the percentage of internalized IRs phosphorylated between 0 and 10 min, as opposed to the gradual decline from 100% to ~70% in the four-pool model. Backer *et al.*[4] showed that the percentage of IRs internalized at 5 min is small [Fig. 5(a)], but the percentage of internalized IRs phosphorylated before 10 min has not been determined [Fig. 5(b)]. What is clear, though, is that the IR models developed here have sufficient structure to determine the proportion of IRs trafficking by these two routes when measurements will be made (see Comparison of the Models section, below).

Parameter estimates for rate constants k_{25}, k_{32}, k_{43}, and k_{54} differ slightly from their four-pool counterparts, which we attribute to the physiologically more accurate structure of the five-pool model.

Six-Pool Model at 100 nM Insulin

Not only are there different predictions for the early time course of the percentage of internalized IRs phosphorylated, for the four-pool, vs. five- and six-pool IR models [Fig. 5(d)], but the six-pool model adds a necessary complexity for determining distinct rates of insulin dissociation and IR dephosphorylation. The half-time for dissociation of insulin from its intracellular receptor in Fao cells is 3 min.[3] Thus, the internalized IRs are free of ligand during much of their intracellular trafficking. Nonetheless, at 20–30 min, when internalization has reached steady state, ~60% of internalized receptors are tyrosine phosphorylated [Fig. 5(d)]. Thus the internalized IR apparently persists in a tyrosine-phosphorylated state after dissociation of its ligand, with a lag of several minutes between insulin dissociation and dephosphorylation of the internalized receptor. In our six-pool model, the rate of internalized IR deactivation in our simpler models is distinguished further into insulin dissociation and IR dephosphorylation. This allows estimation of the rate of IR dephosphorylation, not previously measured in Fao cells, as $k_{56} = 0.101$ min^{-1}, about half as fast as insulin dissociation. This supports previous studies showing that insulin dissociation occurs faster and prior to IR dephosphorylation, and that the IR remains phosphorylated for several minutes following ligand dissociation.[4]

Comparison of the Models

Our four-, five-, and six-pool models all provide similar values for the estimated parameters they have in common (Table 2). Parameter sensitivity analyses (not shown) for all models were consistent with parameter variability estimates (% CVs) for each model optimized parameter. The least sensitive parameters, k_{32} and k_{72}, were the least reliable; however, their % CVs are quite respectable, the worst error being 27.4%.

The AIC for the six-pool model (=2.52) was the lowest, indicating a better fit of the model to data (Table 2). All three models provide similar fits to each data set, however, data set 4 is best fitted by the five-pool and six-pool models, according to objective (least squares) criteria [Fig. 5(d)]. The four-pool model assumes that all IRs are phosphorylated prior to internalization, so at $t \approx 0$ no nonphosphorylated intracellular IRs (x_5) exist and $x_4/(x_4 + x_5) \approx 100$. However, IRs are also internalized in the absence of phosphorylation.[5] The five-pool and six-pool models incorporate the known process of nonphosphorylated IR internalization, to allow $x_4 = 0$ and $x_4 + x_5 + x_7 > 0$ at $t \approx 0$, so the five-pool and six-pool fits to data set 4 begin at 0%. The internalized phosphorylated IR pool has not been measured experimentally before 10 min for 100 nM insulin stimulation, but our three models predict the percentage of internalized IRs phosphorylated during this period. By incorporating known processes of IR activation and nonphosphorylated IR internalization into the Backer *et al.* model, fitting to additional data sets provided up to five additional physiological kinetic parameter estimates.

Four-Pool, Five-Pool, and Six-Pool Model Predictions

To validate our models, we tested the ability of each model to predict data set 6.[4] With all rate constants fixed at their estimated values (Table 2), our four-pool, five-pool, and six-pool models all provided predictive simulations for data set 6. All predictions match the experimental data well, suggesting that the added complexity sufficiently reflects IR trafficking processes.

Our 6-pool model has sufficiently complex structure for examining conditions that could lead to receptor mediated insulin resistance, such as molecular defects in the IR and decreases in IR number,[43] as well as key steps in the termination of the insulin signal in the endosome, such as separate steps for insulin degradation/dissociation and IR dephosphorylation.[19] It has been proposed that activated IR internalization opens a window of time sufficient for phosphorylation of downstream effector molecules participating in the insulin signaling cascade.[19] One of the most important implications resulting from our four-, five-, and

six-pool model predictions is that the internalization of the phosphorylated, activated IR is a rate-limiting step (k_{43}), at least under saturating conditions, possibly not under subsaturating conditions, as previously noted. A decrease in either the amount of IR in a cell or in the rate of IR internalization causes a decrease in the amount of phosphorylated internalized IRs, as expected, and confirmed in our simulations [Fig. 7(a)–7(d)]. Interestingly, decreasing the rate of IR autophosphorylation does not affect steady-state levels of phosphorylated IR [Fig. 7(e) and 7(f)], suggesting that signaling can still continue as long as the IR is capable of being activated.

Understanding the activation dynamics of the surface and endosomal IRs is only part of the framework needed to understand insulin regulated signal transduction. Further dynamic studies are needed to capture the movement of the IR in real time, e.g., the spatiotemporal regulation of IR trafficking. And a more complete framework for understanding insulin signal transduction awaits data linking insulin receptor activation dynamics to postinsulin receptor downstream signaling.

APPENDIX: GLOSSARY OF TERMS

State variables

u = constant insulin input (nM)
x_1 = % of total cellular IRs that are unbound and on the surface
x_2 = % of total cellular IRs that are bound, not phosphorylated and on the surface
x_3 = % of total cellular IRs that are bound, phosphorylated, and on the surface
x_4 = % of total cellular IRs that are bound, phosphorylated, and internalized
x_5 = % of total cellular IRs that are unbound, not phosphorylated, and internalized
x_6 = % of total cellular IRs that are unbound, phosphorylated, and internalized
x_7 = % of total cellular IRs that are bound, not phosphorylated, and internalized

Rate constants

k_{12} = Rate of dissociation of insulin from bound surface IR (nM^{-1} min^{-1})
k_{21} = Rate of insulin association with unbound surface IR (min^{-1})
k_{25} = Rate of deactivated internalized IR recycling (min^{-1})
k_{32} = Rate of surface IR autophosphorylation (min^{-1})
k_{43} = Rate of bound-phosphorylated surface IR internalization (min^{-1})
k_{54} = Rate of deactivation (insulin dissociation and IR dephosphorylation) of internalized IR (min^{-1})
k_{56} = Rate of dephosphorylation of internalized IR (min^{-1})
k_{57} = Rate of dissociation of insulin from bound-nonphosphorylated internalized IR (min^{-1})
k_{64} = Rate of dissociation of insulin from bound-phosphorylated internalized IR (min^{-1})
k_{72} = Rate of internalization of bound-nonphosphorylated surface IR (min^{-1})

Initial conditions

$x_1(0) = 100\%$
$x_i = 0$ for $i \neq 1$

ACKNOWLEDGMENTS

This investigation was supported in part by a National Institutes of Health (NIH), National Institute of General Medical Sciences (NIGMS), GM008185 to SSH, an NIH, National Institute of Diabetes and Digestive and Kidney Diseases (NIDDK), R01 DK58132 to IJK and NIH-NIDDK R01 DK34839 to JJD.

REFERENCES

[1] Akaike, H. A new look at the statistical model identification. *IEEE Trans. Autom. Control* AC-19:716–723, 1974.
[2] Authier, F., M. Metioui, S. Fabrega, M. Kouach, and G. Briand. Endosomal proteolysis of internalized insulin at the C-terminal region of the B chain by cathepsin D. *J. Biol. Chem.* 277:9437–9446, 2002.
[3] Backer, J. M., C. R. Kahn, and M. F. White. The dissociation and degradation of internalized insulin occur in the endosomes of rat hepatoma cells. *J. Biol. Chem.* 265:14828–14835, 1990.
[4] Backer, J. M., C. R. Kahn, M. F. White. Tyrosine phosphorylation of the insulin receptor during insulin-stimulated internalization in rat hepatoma cells. *J. Biol. Chem.* 264:1694–1701, 1989.
[5] Backer, J. M., C. R. Kahn, and M. F. White. Tyrosine phosphorylation of the insulin receptor is not required for receptor internalization: studies in 2,4-dinitrophenol-treated cells. *Proc. Natl. Acad. Sci. USA* 86:3209–3213, 1989.
[6] Backer, J. M., S. E. Shoelson, E. Haring, and M. F. White. Insulin receptors internalize by a rapid, saturable pathway requiring receptor autophosphorylation and an intact juxtamembrane region. *J. Cell. Biol.* 115:1535–1545, 1991.
[7] Balbis, A., G. Baquiran, J. J. Bergeron, and B. I. Posner. Compartmentalization and insulin-induced translocations of insulin receptor substrates, phosphatidylinositol 3-kinase, and protein kinase B in rat liver. *Endocrinology* 141:4041–4049, 2000.
[8] Balbis, A., G. Baquiran, V. Dumas, and B. I. Posner. Effect of inhibiting vacuolar acidification on insulin signaling in hepatocytes. *J. Biol. Chem.* 279:12777–12785, 2004.
[9] Ballotti, R., A. Kowalski, M. F. White, Y. Le Marchand-Brustel, and E. Van Obberghen. Insulin stimulates tyrosine phosphorylation of its receptor beta-subunit in intact rat hepatocytes. *Biochem. J.* 241:99–104, 1987.
[10] Barrett, P. H., B. M. Bell, C. Cobelli, H. Golde, A. Schumitzky, P. Vicini, and D. M. Foster. SAAM II: Simulation, Analysis, and Modeling Software for tracer and pharmacokinetic studies. *Metabolism* 47:484–492, 1998.
[11] Bell, B. M., J. V. Burke, and A. Schumitzky. A relative weighting method for estimating parameters and variances in multiple data sets. *Comp. Stat. Data Anal.* 22:119–135, 1996.
[12] Bergeron, J. J., J. Cruz, M. N. Khan, and B. I. Posner. Uptake of insulin and other ligands into receptor-rich endocytic components of target cells: the endosomal apparatus. *Annu. Rev. Physiol.* 47:383–403, 1985.
[13] Bevan, A. P., P. J. Seabright, J. Tikerpae, B. I. Posner, G. D. Smith, and K. Siddle. The role of insulin dissociation from its endosomal receptor in insulin degradation. *Mol. Cell Endocrinol.* 164:145–157, 2000.
[14] Bruning, J. C., M. D. Michael, J. N. Winnay, T. Hayashi, D. Horsch, D. Accili, L. J. Goodyear, and C. R. Kahn. A muscle-specific insulin receptor knockout exhibits features of the metabolic syndrome of NIDDM without altering glucose tolerance. *Mol. Cell.* 2:559–569, 1998.

[15]Cheng, A., N. Dube, F. Gu, and M. L. Tremblay. Coordinated action of protein tyrosine phosphatases in insulin signal transduction. *Eur. J. Biochem*. 269:1050–1059, 2002.

[16]Cobelli, C., and J. J. DiStefano III. Parameter and structural identifiability concepts and ambiguities: A critical review and analysis. *Am. J. Physiol*. 239:R7–R24, 1980.

[17]Contreres, J. O., R. Faure, G. Baquiran, J. J. Bergeron, and B. I. Posner. ATP-dependent desensitization of insulin binding and tyrosine kinase activity of the insulin receptor kinase. The role of endosomal acidification. *J. Biol. Chem*. 273:22007–22013, 1998.

[18]Crettaz, M., and C. R. Kahn. Analysis of insulin action using differentiated and dedifferentiated hepatoma cells. *Endocrinology* 113:1201–1209, 1983.

[19]Di Guglielmo, G. M., P. G. Drake, P. C. Baass, F. Authier, B. I. Posner, and J. J. Bergeron. Insulin receptor internalization and signalling. *Mol. Cell Biochem*. 182:59–63, 1998.

[20]Drake, P. G., and B. I. Posner. Insulin receptor-associated protein tyrosine phosphatase(s): Role in insulin action. *Mol. Cell Biochem*. 182:79–89, 1998.

[21]Faure, R., G. Baquiran, J. J. Bergeron, and B. I. Posner. The dephosphorylation of insulin and epidermal growth factor receptors. Role of endosome-associated phosphotyrosine phosphatase(s). *J. Biol. Chem*. 267:11215–11221, 1992.

[22]Galic, S., C. Hauser, B. B. Kahn, F. G. Haj, B. G. Neel, N. K. Tonks, and T. Tiganis. Coordinated regulation of insulin signaling by the protein tyrosine phosphatases PTP1B and TCPTP. *Mol. Cell Biol*. 25:819–829, 2005.

[23]Galic, S., M. Klingler-Hoffmann, M. T. Fodero-Tavoletti, M. A. Puryer, T. C. Meng, N. K. Tonks, and T. Tiganis. Regulation of insulin receptor signaling by the protein tyrosine phosphatase TCPTP. *Mol. Cell Biol*. 23:2096–2108, 2003.

[24]Gammeltoft, S., L. O. Kristensen, and L. Sestoft. Insulin receptors in isolated rat hepatocytes. Reassessment of binding properties and observations of the inactivation of insulin at 37 degrees C. *J. Biol. Chem*. 253:8406–8413, 1978.

[25]Gill, G. N. A pit stop at the ER. *Science*. 295:1654–1655, 2002.

[26]Haj, F. G., P. J. Verveer, A. Squire, B. G. Neel, and P. I. Bastiaens. Imaging sites of receptor dephosphorylation by PTP1B on the surface of the endoplasmic reticulum. *Science* 295:1708–1711, 2002.

[27]Haj, F. G., J. M. Zabolotny, Y. B. Kim, B. B. Kahn, and B. G. Neel. Liver specific protein-tyrosine phosphatase 1B (PTP1B) Re-expression alters glucose homeostasis of PTP1B-/-mice. *J. Biol. Chem*. 2005.

[28]Haring, H. U., M. Kasuga, M. F. White, M. Crettaz, and C. R. Kahn. Phosphorylation and dephosphorylation of the insulin receptor: evidence against an intrinsic phosphatase activity. *Biochemistry* 23:3298–3306, 1984.

[29]Issad, T., N. Boute, S. Boubekeur, and D. Lacasa. Interaction of PTPB with the insulin receptor precursor during its biosynthesis in the endoplasmic reticulum. *Biochemistry* 87:111–116, 2005.

[30]Kasuga, M., F. A. Karlsson, and C. R. Kahn. Insulin stimulates the phosphorylation of the 95,000-dalton subunit of its own receptor. *Science* 215:185–187, 1982.

[31]Knutson, V. P.. Cellular trafficking and processing of the insulin receptor. *FASEB J*. 5:2130–2138, 1991.

[32]Lauffenburger, D. A., and J. J. Linderman. Receptors: Models for Binding, Trafficking, and Signaling. New York: Oxford University Press, 1993, pp. 365.

[33]Meng, T. C., D. A. Buckley, S. Galic, T. Tiganis, and N. K. Tonks. Regulation of insulin signaling through reversible oxidation of the protein-tyrosine phosphatases TC45 and PTP1B. *J. Biol. Chem*. 279:37716–37725, 2004.

[34]Peck, C. C., S. L. Beal, L. B. Sheiner, and A. I. Nichols. Extended least squares nonlinear regression: A possible solution to the "choice of weights" problem in analysis of individual pharmacokinetic data. *J. Pharmacokinet. Biopharmacol*. 12:545–558, 1984.

[35]Peck, C. C., L. B. Sheiner, and A. I. Nichols. The problem of choosing weights in nonlinear regression analysis of pharmacokinetic data. *Drug Metab. Rev*. 15:133–148, 1984.

[36]Perz, M., and T. Torlinska. Insulin receptor–structural and functional characteristics. *Med. Sci. Monitor* 7:169–177, 2001.

[37]Posner, B. I.. Regulation of insulin receptor kinase activity by endosomal processes: possible areas for therapeutic intervention. *Curr. Opin. Investig. Drugs* 4:430–434, 2003.

[38]Quon, M. J., and L. A. Campfield. A mathematical model and computer simulation study of insulin receptor regulation. *J. Theor. Biol*. 150:59–72, 1991.

[39]Romsicki, Y., M. Reece, J. Y. Gauthier, E. Asante-Appiah, and B. P. Kennedy. Protein tyrosine phosphatase-1B dephosphorylation of the insulin receptor occurs in a perinuclear endosome compartment in human embryonic kidney 293 cells. *J. Biol. Chem*. 279:12868–12875, 2004.

[40]Schranz, D. B., A. M. Rohilla, C. Anderson, W. M. Wood, and P. Berhanu. Insulin internalization in the absence of the insulin receptor tyrosine kinase domain is insufficient for mediating intracellular biological effects. *Biochem. Biophys. Res. Commun*. 227:600–607, 1996.

[41]Seber, G. A. F., and C. J. Wild. Nonlinear Regression. Hoboken: Wiley, 2003, pp. 768.

[42]Sedaghat, A. R., A. Sherman, and M. J. Quon. A mathematical model of metabolic insulin signaling pathways. *Am. J. Physiol. Endocrinol. Metab*. 283:E1084–E1101, 2002.

[43]Sesti, G., M. Federici, D. Lauro, P. Sbraccia, and R. Lauro. Molecular mechanism of insulin resistance in type 2 diabetes mellitus: Role of the insulin receptor variant forms. *Diabetes Metab. Res. Rev*. 17:363–373, 2001.

[44]White, M. F., H. U. Haring, M. Kasuga, and C. R. Kahn. Kinetic properties and sites of autophosphorylation of the partially purified insulin receptor from hepatoma cells. *J. Biol. Chem*. 259:255–264, 1984.